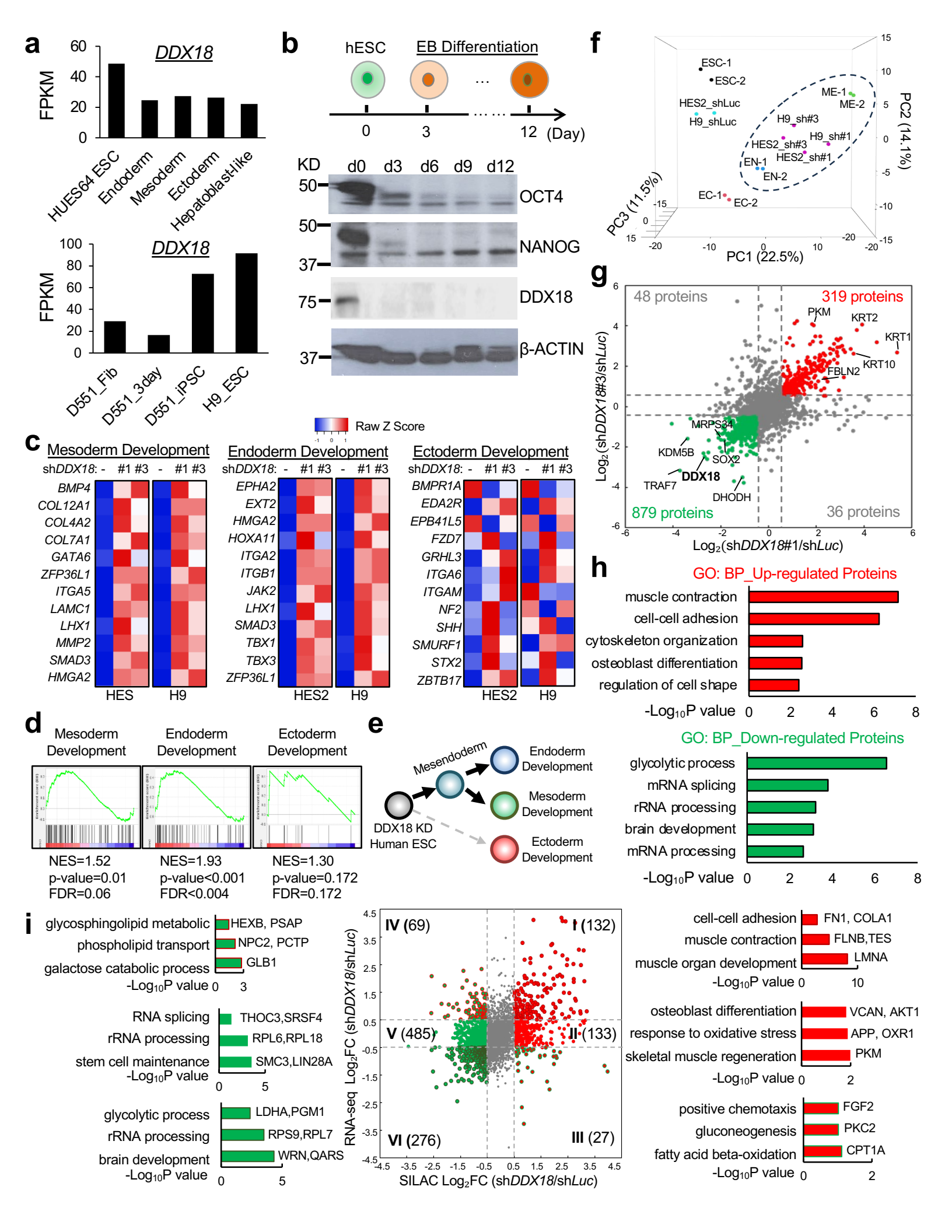
a
DDX18
FPKM
HUES64 ESC
Endoderm
Mesoderm
Ectoderm
Hepatoblast-like
DDX18
D551_Fib
D551_3day
D551_iPSC
H9_ESC
b
hESC
EB Differentiation
0
3
12 (Day)
KD
d0 d3 d6 d9 d12
OCT4
NANOG
DDX18
β-ACTIN
f
ESC-1
ESC-2
ME-1
ME-2
HES2_shLuc
H9_shLuc
H9_sh#3
H9_sh#1
HES2_sh#3
HES2_sh#1
EN-1
EN-2
EC-1
EC-2
PC1 (22.5%)
PC2 (14.1%)
PC3 (11.5%)
g
48 proteins
319 proteins
879 proteins
36 proteins
PKM
KRT2
KRT1
KRT10
FBLN2
MRPS34
KDM5B
SOX2
DDX18
TRAF7
DHODH
Log2(shDDX18#3/shLuc)
Log2(shDDX18#1/shLuc)
c
Raw Z Score
Mesoderm Development
Endoderm Development
Ectoderm Development
shDDX18: - #1 #3 - #1 #3
BMP4
COL12A1
COL4A2
COL7A1
GATA6
ZFP36L1
ITGA5
LAMC1
LHX1
MMP2
SMAD3
HMGA2
EPHA2
EXT2
HMGA2
HOXA11
ITGA2
ITGB1
JAK2
LHX1
SMAD3
TBX1
TBX3
ZFP36L1
BMPR1A
EDA2R
EPB41L5
FZD7
GRHL3
ITGA6
ITGAM
NF2
SHH
SMURF1
STX2
ZBTB17
HES
H9
HES2
H9
HES2
H9
h
GO: BP_Up-regulated Proteins
muscle contraction
cell-cell adhesion
cytoskeleton organization
osteoblast differentiation
regulation of cell shape
-Log10P value
GO: BP_Down-regulated Proteins
glycolytic process
mRNA splicing
rRNA processing
brain development
mRNA processing
-Log10P value
d
Mesoderm Development
Endoderm Development
Ectoderm Development
NES=1.52
p-value=0.01
FDR=0.06
NES=1.93
p-value<0.001
FDR<0.004
NES=1.30
p-value=0.172
FDR=0.172
e
Mesendoderm
DDX18 KD
Human ESC
Endoderm Development
Mesoderm Development
Ectoderm Development
i
glycosphingolipid metabolic
phospholipid transport
galactose catabolic process
HEXB, PSAP
NPC2, PCTP
GLB1
-Log10P value
RNA splicing
rRNA processing
stem cell maintenance
THOC3,SRSF4
RPL6,RPL18
SMC3,LIN28A
-Log10P value
glycolytic process
rRNA processing
brain development
LDHA,PGM1
RPS9,RPL7
WRN,QARS
-Log10P value
IV (69)
I (132)
V (485)
II (133)
VI (276)
III (27)
RNA-seq Log2FC (shDDX18/shLuc)
SILAC Log2FC (shDDX18/shLuc)
cell-cell adhesion
muscle contraction
muscle organ development
FN1, COLA1
FLNB,TES
LMNA
-Log10P value
osteoblast differentiation
response to oxidative stress
skeletal muscle regeneration
VCAN, AKT1
APP, OXR1
PKM
-Log10P value
positive chemotaxis
gluconeogenesis
fatty acid beta-oxidation
FGF2
PKC2
CPT1A
-Log10P value

Supplementary Fig. S1 | DDX18 is required for pluripotency maintenance.

a, Relative expression of *DDX18* in human ESCs (HUES64) relative to their differentiated lineages[1] (top) and during the reprogramming of Detroit 551 (D551) fibroblasts toward iPSCs[2] (bottom). Data were extracted from RNA-seq datasets in the public domains as specified.

b, Western blot analysis confirming the marked reduction of OCT4, NANOG, and DDX18 proteins upon EB differentiation of hESCs. β-ACTIN serves as the loading control. Asterisks indicate non-specific (ns) bands.

c, Heatmaps of expression changes of RNA following DDX18 depletion. Representative genes associated with mesoderm, endoderm, and ectoderm genes are shown.

d, Geneset Enrichment Analysis (GSEA) of the three lineages in DDX18 KD vs. control hESCs.

e, Human ESCs are skewed to mesendoderm differentiation upon DDX18 depletion.

f, Principal-component analysis (PCA) comparing the transcriptome of this study with those from published datasets[3].

g, SILAC-MS results showing protein expression ratios in control relative to DDX18 KD cells, X and Y axes represent the data from sh*DDX18*#1 and sh*DDX18*#3, respectively. The dashed lines indicate the data cut-off criterion Log_2 [fold change] <-0.5 or >0.5.

h, GO analysis of significantly up- and down-regulated proteins upon DDX18 KD in hESCs.

i, Scatter plot of the expression changes of proteins and mRNAs following DDX18 KD (sh*DDX18*, an average value from two replicates of sh*DDX18*#1 and sh*DDX18*#3) relative to control KD (sh*Luc*). Six different groups of genes are plotted. GO analyses of each group are shown. Representative genes of each GO term are also listed beside the bar.

Source data are provided as a Source Data file.

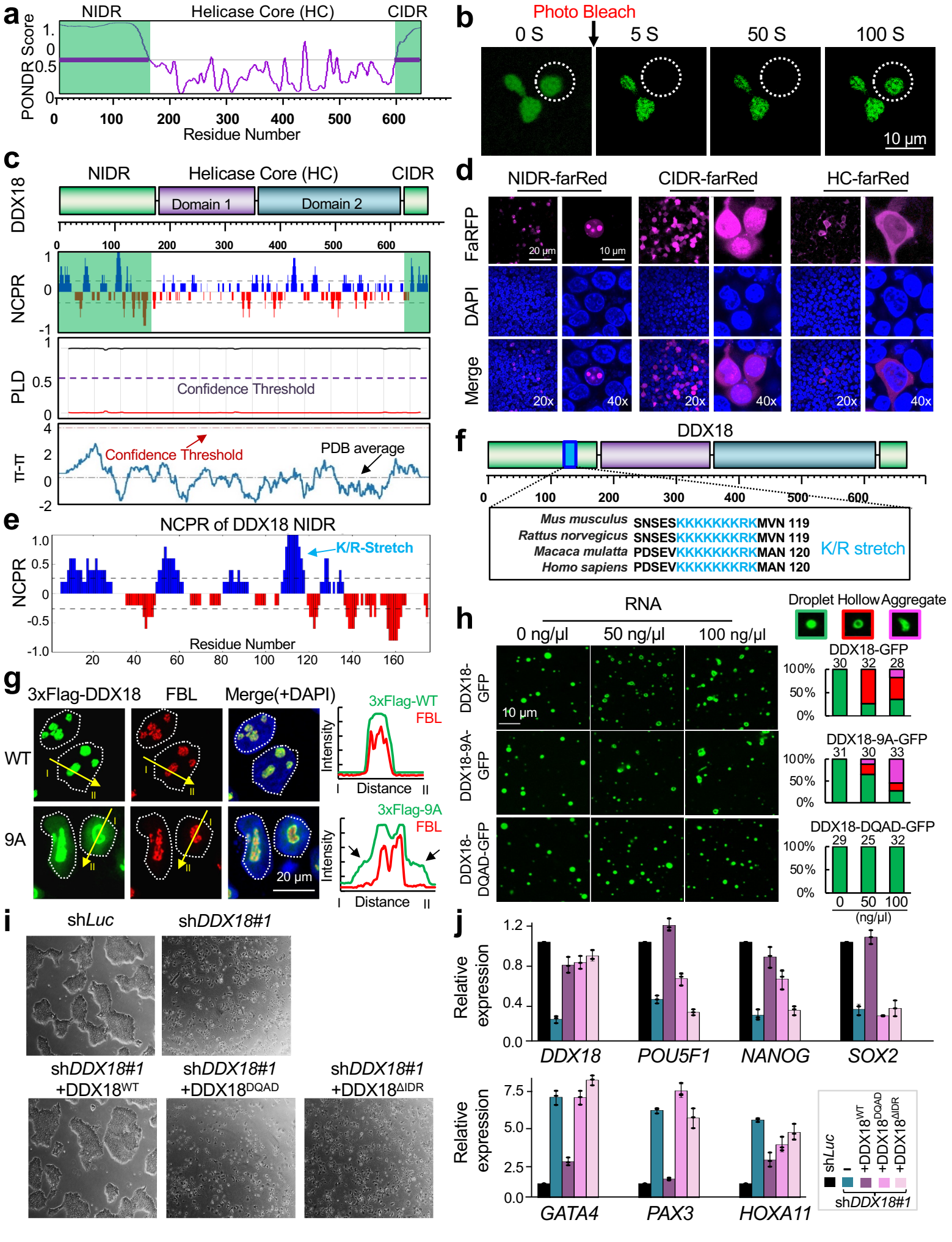
a
NIDR
Helicase Core (HC)
CIDR
PONDR Score
Residue Number
b
Photo Bleach
0 S
5 S
50 S
100 S
10 μm
c
DDX18
Domain 1
Domain 2
NCPR
PLD
Confidence Threshold
π-π
PDB average
d
NIDR-farRed
CIDR-farRed
HC-farRed
FaRFP
DAPI
Merge
20 μm
10 μm
20x
40x
e
NCPR of DDX18 NIDR
K/R-Stretch
f
DDX18
Mus musculus SNSESKKKKKKKRKMVN 119
Rattus norvegicus SNSESKKKKKKKRKMVN 119
Macaca mulatta PDSEVKKKKKKKRKMAN 120
Homo sapiens PDSEVKKKKKKKRKMAN 120
K/R stretch
g
3xFlag-DDX18
FBL
Merge(+DAPI)
WT
9A
3xFlag-WT
FBL
3xFlag-9A
FBL
Intensity
Distance
20 μm
h
RNA
0 ng/μl
50 ng/μl
100 ng/μl
Droplet
Hollow
Aggregate
DDX18-GFP
DDX18-9A-GFP
DDX18-DQAD-GFP
10 μm
(ng/μl)
i
shLuc
shDDX18#1
shDDX18#1 +DDX18WT
shDDX18#1 +DDX18DQAD
shDDX18#1 +DDX18ΔIDR
j
Relative expression
DDX18
POU5F1
NANOG
SOX2
GATA4
PAX3
HOXA11
shLuc
+DDX18WT
+DDX18DQAD
+DDX18ΔIDR
shDDX18#1

Supplementary Fig. S2 | DDX18 undergoes phase separation *in vitro* and *in vivo*.

a, Graph plot showing the intrinsic disorder (PONDR VSL2) for DDX18. PONDR VSL2 score (Y-axis) and amino acid position (X-axis) are shown. The purple bar designates the IDR under investigation.

b, Representative images showing FRAP of DDX18-GFP. Photo bleach was performed at t = 0 s.

c, Prion-like domains (PLD), propensity for π-π contacts (π-π), the fraction of charged residues, and net charge per residues (NCPR) prediction are shown. Residue numbers corresponding to DDX18 are shown on the top.

d, Immunostaining of DDX18 domains fused with FarRed in 293T cells. The nucleus is stained with DAPI. Images were taken at two (20x and 40x) magnifications for each sample.

e, NCPR of DDX18 NIDR (1-175 amino acid). K-stretch within NIDR was indicated.

f, DDX18 contains a Lysine (K) stretch in its N terminal IDR, which is highly conserved among multiple species.

g, Representative images and quantification of the nucleoplasm localization of DDX18-WT and DDX18-9A mutant in hESCs. DDX18-WT is highly enriched in the nucleolus, and FBL is a nucleolus marker. The right-most panels show the quantified intensity of 3xFlag-WT, 3xFlag-9A (green), or FBL (red) immunofluorescence signals along the yellow lines in the left images. Arrows indicate that 3xFlag-9A is localized outside of the nucleolus.

h, Left: Representative images of the mixtures of equal amounts (10 μM) of DDX18-GFP, DDX18-9A-GFP, and DDX18-DQAD-GFP recombinant proteins with total RNAs from 293T cells under various concentrations indicated in a buffer comprised of 150 mM NaCl, 25 mM Tris-HCl, pH 8.0. Right: Quantification of representative structures of the mixtures from *in vitro* droplet forming assays (percentages of the representative structures from WT and mutant recombinant proteins are quantified and plotted). Total droplets counted under respective RNA concentrations were shown on top of bars.

i, Phase-contrast images showing that hESC differentiation by DDX18 KD cannot be rescued by IDR deletion or RNA helicase mutant of DDX18.

j, RT-qPCR analysis showing DDX18 IDR deletion or RNA helicase mutant of DDX18 does not rescue the expression of pluripotency genes. Data were obtained from two biological replicates and presented as Mean ± SD.

Source data are provided as a Source Data file.

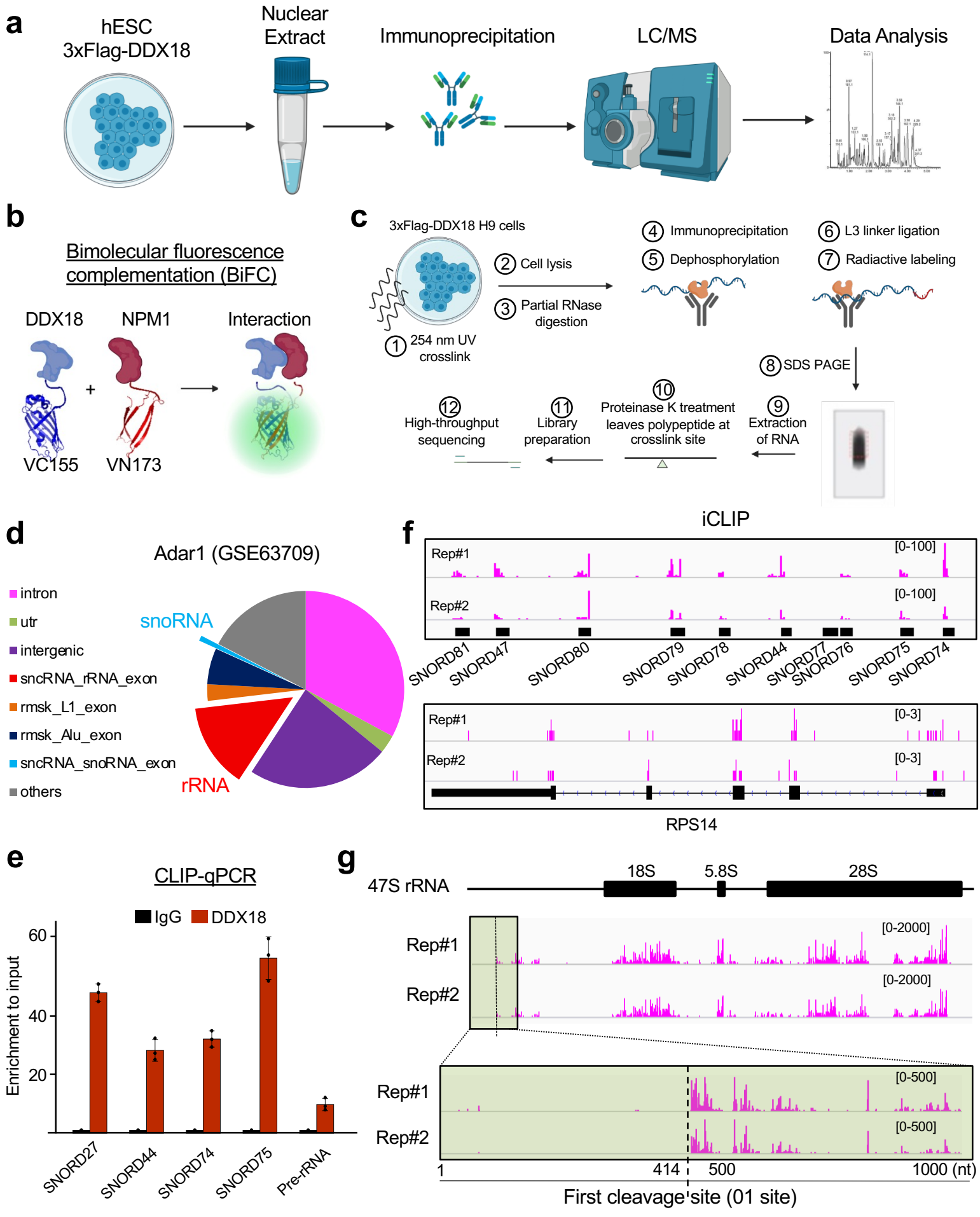
a
hESC
3xFlag-DDX18
Nuclear
Extract
Immunoprecipitation
LC/MS
Data Analysis
b
Bimolecular fluorescence
complementation (BiFC)
DDX18
NPM1
Interaction
VC155
VN173
c
3xFlag-DDX18 H9 cells
1 254 nm UV
crosslink
2 Cell lysis
3 Partial RNase
digestion
4 Immunoprecipitation
5 Dephosphorylation
6 L3 linker ligation
7 Radiactive labeling
8 SDS PAGE
9 Extraction
of RNA
10 Proteinase K treatment
leaves polypeptide at
crosslink site
11 Library
preparation
12 High-throughput
sequencing
d
Adar1 (GSE63709)
intron
utr
intergenic
sncRNA_rRNA_exon
rmsk_L1_exon
rmsk_Alu_exon
sncRNA_snoRNA_exon
others
snoRNA
rRNA
f
iCLIP
Rep#1
Rep#2
[0-100]
[0-100]
SNORD81
SNORD47
SNORD80
SNORD79
SNORD78
SNORD44
SNORD77
SNORD76
SNORD75
SNORD74
[0-3]
[0-3]
RPS14
e
CLIP-qPCR
IgG
DDX18
Enrichment to input
60
40
20
SNORD27
SNORD44
SNORD74
SNORD75
Pre-rRNA
g
47S rRNA
18S
5.8S
28S
Rep#1
Rep#2
[0-2000]
[0-2000]
[0-500]
[0-500]
1
414
500
1000 (nt)
First cleavage site (01 site)

Supplementary Fig. S3 | DDX18 interacts with nucleolar RNAs and GC component proteins.
a, Schematic diagram of IP-MS procedure. Nuclear extracts from 3xFlag-DDX18 hESCs were used for immunoprecipitation.
b, Schematic depiction of BiFC to detect the specific interaction of DDX18 with NPM1.
c, Schematic depiction of the iCLIP procedure.
d, Relative enrichment of different RNA species in Adar1 iCLIP-seq from GSE63709.
e, CLIP-qPCR analysis of indicated snoRNAs from a single experimental test.
f, IGV snapshots of DDX18 iCLIP-seq on snoRNAs and mRNA (RPS14) locus.
g, CLIP peaks showing the weak DDX18 binding signal at the 5'ETS (1∼414 nt) of 47S pre-rRNAs.
a, **b**, and **c** were created in BioRender. Malik, V. (2025) https://BioRender.com/v27l155
Source data are provided as a Source Data file.

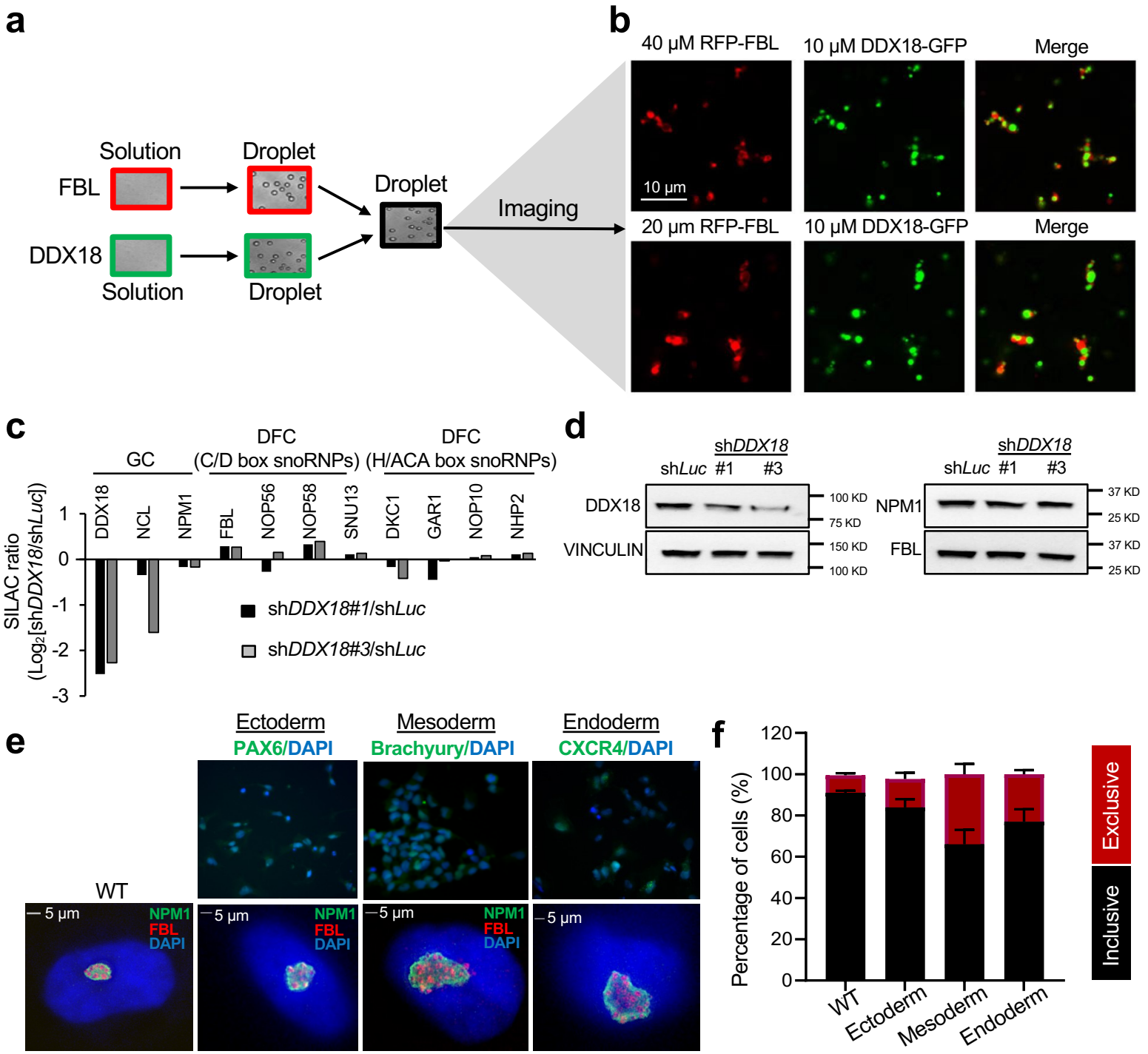
a
Solution
Droplet
FBL
Droplet
DDX18
Solution
Droplet
Imaging
b
40 μM RFP-FBL
10 μM DDX18-GFP
Merge
10 μm
20 μm RFP-FBL
10 μM DDX18-GFP
Merge
c
GC
DFC
(C/D box snoRNPs)
DFC
(H/ACA box snoRNPs)
DDX18
NCL
NPM1
FBL
NOP56
NOP58
SNU13
DKC1
GAR1
NOP10
NHP2
SILAC ratio
(Log2[shDDX18/shLuc])
1
0
-1
-2
-3
shDDX18#1/shLuc
shDDX18#3/shLuc
d
shDDX18
shLuc #1 #3
DDX18
VINCULIN
100 KD
75 KD
150 KD
100 KD
shDDX18
shLuc #1 #3
NPM1
FBL
37 KD
25 KD
37 KD
25 KD
e
Ectoderm
PAX6/DAPI
Mesoderm
Brachyury/DAPI
Endoderm
CXCR4/DAPI
WT
5 μm
NPM1
FBL
DAPI
f
Percentage of cells (%)
120
100
80
60
40
20
0
WT
Ectoderm
Mesoderm
Endoderm
Exclusive
Inclusive

Supplementary Fig. S4 | Architecture of the nucleolus arises through multiphase liquid miscibility and immiscibility of DDX18 with NPM1 and FBL, respectively.

a-b, Experimental strategy (**a**) and representative images (**b**) of the mixtures of DDX18-GFP droplets with RFP-FBL droplets in a buffer comprised of 150 mM NaCl, 25 mM Tris-HCl, pH 8.0.

c, SILAC data showing nucleolar proteins are unchanged upon DDX18 KD.

d, Western blot analysis with anti-FBL, anti-DDX18, anti-NPM1, and anti-VINCULIN antibodies confirming that DDX18 KD does not affect NPM1 and FBL protein expression levels.

e, The detection of nucleolar caps during hESC differentiation. Human ESCs were differentiated into three primary germ layers using the STEMdiffTM Trilineage Differentiation Kit. Top panels: Immunofluorescence microscopy images of three lineage markers (top panel); Bottom panels: SIM confocal microscopy images of nucleolar condensate organization in wildtype and differentiated hESCs. FBL labels the dense fibrillar component (DFC), and NPM1 labels the granular component (GC).

f, Quantification of immunofluorescence microscopy images shown in f. The percentages of inclusive or exclusive DFC cells were quantified from at least 20 cells of WT and each of the three lineages.

Source data are provided as a Source Data file.

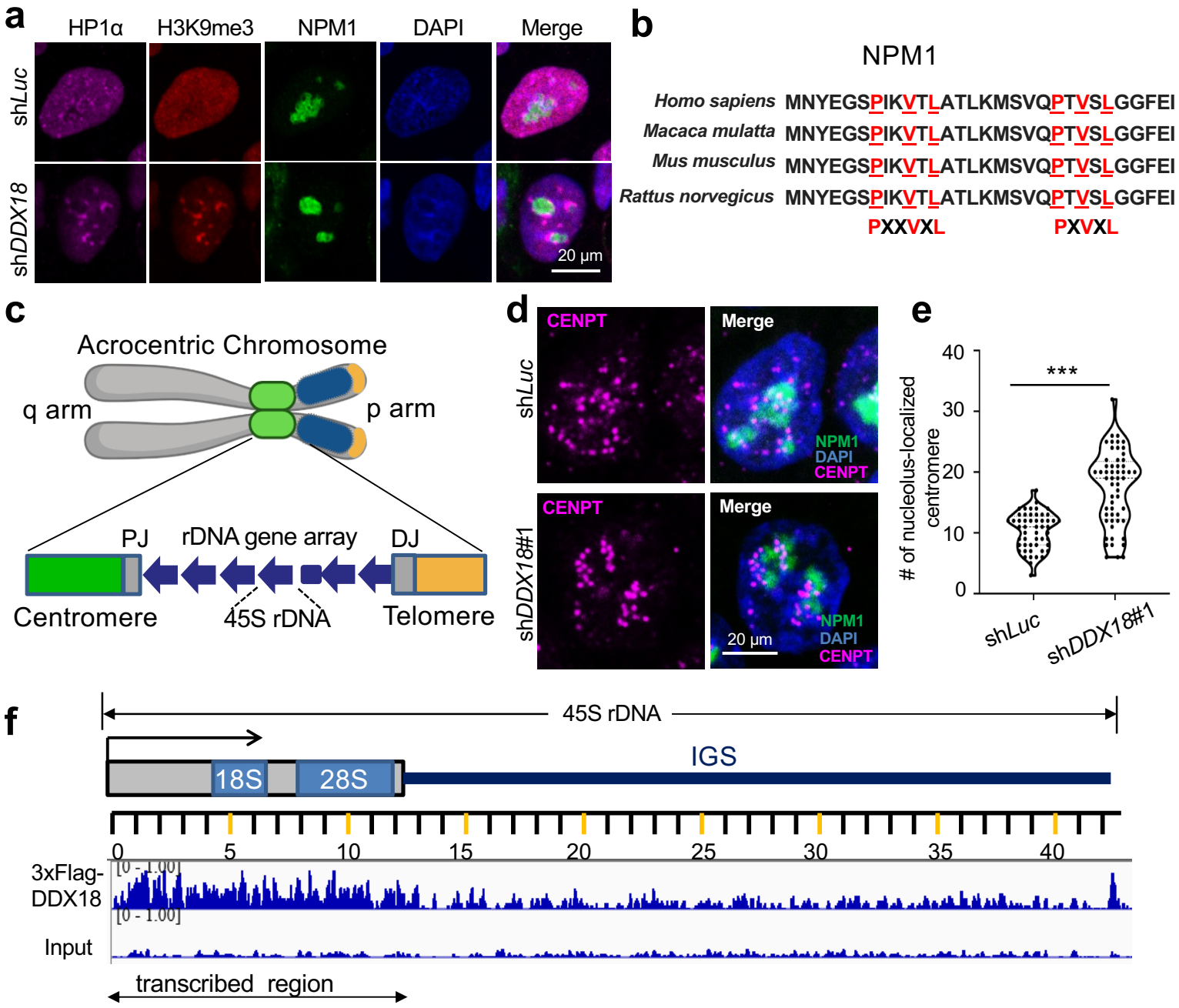
a
HP1α
H3K9me3
NPM1
DAPI
Merge
shLuc
shDDX18
20 μm
b
NPM1
Homo sapiens MNYEGSPIKVTLATLKMSVQPTVSLGGFEI
Macaca mulatta MNYEGSPIKVTLATLKMSVQPTVSLGGFEI
Mus musculus MNYEGSPIKVTLATLKMSVQPTVSLGGFEI
Rattus norvegicus MNYEGSPIKVTLATLKMSVQPTVSLGGFEI
PXXVXL
PXVXL
c
Acrocentric Chromosome
q arm
p arm
PJ
rDNA gene array
DJ
Centromere
45S rDNA
Telomere
d
CENPT
Merge
shLuc
shDDX18#1
NPM1
DAPI
CENPT
20 μm
e
# of nucleolus-localized centromere
***
shLuc
shDDX18#1
f
45S rDNA
IGS
18S
28S
3xFlag-DDX18
Input
transcribed region

Supplementary Fig. S5 | DDX18 KD disrupted nucleolar structure leading to perinucleolar heterochromatin organization.

a, Immunofluorescence showing heterochromatin (H3K9me3) and nucleoli (NPM1) of control and DDX18 KD hESCs.

b, Protein sequence analysis showing two evolutionarily conserved HP1α binding motifs in NPM1.

c, Schematic diagram showing the organization structure of an acrocentric chromosome. (Created in BioRender. Malik, V. (2025) https://BioRender.com/v27l155)

d, Immunofluorescence showing centromere clustering closer to nucleoli (NPM1) in DDX18 KD than control hESCs.

e, Quantification of the numbers of centromere foci around nucleolus from more than 50 cells. Each dot represents one cell. ***P < 0.001.

f, IGV snapshots of DDX18 ChIP-seq on 45S rDNA reference genome assembly (see Methods for mapping description).

Source data are provided as a Source Data file.

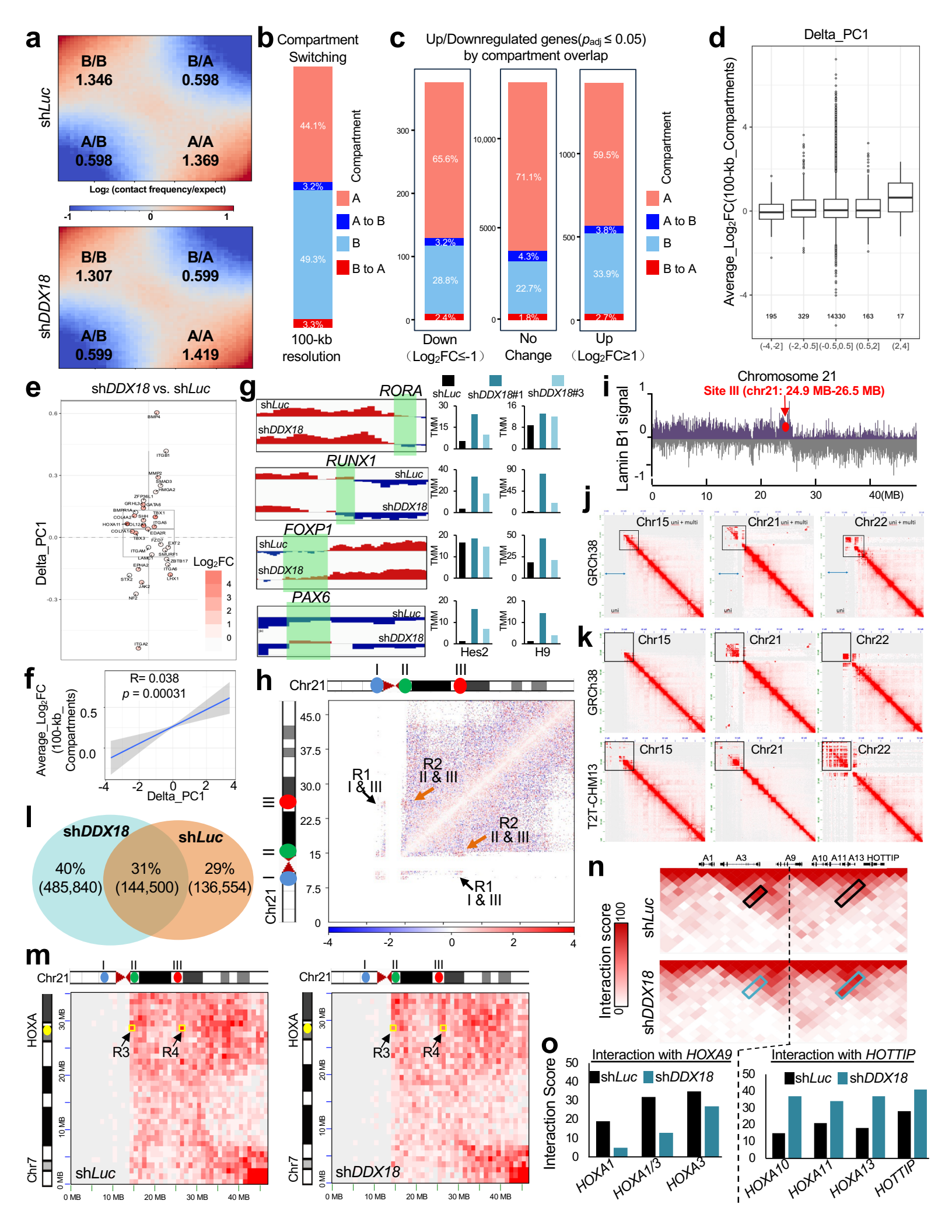
a
shLuc
B/B 1.346
B/A 0.598
A/B 0.598
A/A 1.369
Log2 (contact frequency/expect)
-1
0
1
shDDX18
B/B 1.307
B/A 0.599
A/B 0.599
A/A 1.419
b
Compartment Switching
44.1%
3.2%
49.3%
3.3%
Compartment
A
A to B
B
B to A
100-kb resolution
c
Up/Downregulated genes(padj ≤ 0.05) by compartment overlap
65.6%
3.2%
28.8%
2.4%
71.1%
4.3%
22.7%
1.8%
59.5%
3.8%
33.9%
2.7%
Down (Log2FC≤-1)
No Change
Up (Log2FC≥1)
d
Delta_PC1
Average_Log2FC(100-kb_Compartments)
195
329
14330
163
17
(-4,-2]
(-2,-0.5]
(-0.5,0.5]
(0.5,2]
(2,4]
e
shDDX18 vs. shLuc
Delta_PC1
Log2FC
f
R= 0.038
p = 0.00031
Average_Log2FC (100-kb_Compartments)
Delta_PC1
g
RORA
RUNX1
FOXP1
PAX6
shLuc
shDDX18
shDDX18#1
shDDX18#3
TMM
Hes2
H9
h
Chr21
R1 I & III
R2 II & III
i
Chromosome 21
Site III (chr21: 24.9 MB-26.5 MB)
Lamin B1 signal
40(MB)
j
Chr15
Chr21
Chr22
GRCh38
k
T2T-CHM13
l
shDDX18
shLuc
40% (485,840)
31% (144,500)
29% (136,554)
m
HOXA
Chr7
R3
R4
shLuc
shDDX18
n
A1
A3
A9
A10
A11
A13
HOTTIP
Interaction score
o
Interaction with HOXA9
Interaction with HOTTIP
Interaction Score
HOXA1
HOXA1/3
HOXA3
HOXA10
HOXA11
HOXA13
HOTTIP

Supplementary Fig. S6 | Depletion of DDX18 results in chromatin reorganization and HOXA gene derepression.

a, Saddle plots of Hi-C data binned at 100-kb resolution showing decreased B-B compartment strength and increased A-A compartment strength in DDX18 KD (sh*DDX18*) relative to control KD (sh*Luc*) hESCs.

b, Quantitative analysis of the compartment switch in control and DDX18 KD Hi-C data, with A and B compartments classified based on eigenvector values (PC1) from PCA analysis.

c, The relationship between transcription and compartment organization from the integrative analysis of Hi-C sequencing combined with RNA sequencing, revealing that only a small proportion of bins showing extreme changes in PC1 values (±2) correlated with significant gene up- or down-regulation.

d, A box plot displaying the average gene expression changes associated with eigenvector values (PC1) changes, with the number of genes labeled below the box. Positive and negative changes in PC1 values are expected to imply a shift towards active and inactive transcriptional states, respectively.

e, A scatter plot showing the correlation of genes with a significant increase in expression with an increased PC1 value.

f, A global analysis of the correlation between gene expression changes and PC1 value changes.

g, Compartment switch of *RORA*, *RUNX1*, *PAX6*, and *FOXP1* genes displayed by IGV snapshots (left) and their relative RNA expression levels (from RNA-seq data the trimmed mean of M values; TMM) depicted by bar charts (right) between control and DDX18 KD hESCs.

h, Differential contact heatmap showing increased contact frequency of region 1 (R1) and region 2 (R2).

i, Lamin B1 contacting analysis of a public dataset[4] showing the site III is a LAD gene locus in wildtype hESCs.

j, Hi-C matrices (250-kb resolution) of control KD cells showing raw interaction counts based on uniquely mapping reads (bottom left) or unique and multimapping reads (top right). Black boxes highlight regions with significant rescue of multimapping reads. Blue arrows show gaps in the short arms in the reference genome GRCh38.

k, Hi-C matrices (250-kb resolution) of control KD cells showing raw interaction counts generated from mHi-C pipeline using GRCh38 (top) or T2T-CHM13 (bottom) reference genome. Black boxes highlight regions showing significant reduction in gaps in T2T-CHM13 reference genome.

l, Number of significant interactions detected in DDX18 KD and control KD samples.

m, Contact heatmaps showing weakened interactions of *HOXA* cluster genes on Chr7 with the pericentromeric locus (Site II, Chr21: 14.7 MB-15.1 MB) (R3) and the chromosome arm locus (Site III, Chr21: 24.9 MB-26.5 MB) (R4) in DDX18 KD relative to control KD hESCs.

n,**o**, Contact heatmaps showing weakened and enhanced interactions in the internal (left) and external (right) *HOXA* cluster genes, respectively, in DDX18 KD (sh*DDX18*, blue boxes) relative to control KD (sh*Luc*, black boxes) hESCs (**n**) and bar charts depicting their quantifications (**o**). *HOXA1/3* denotes the internal interaction of the genomic region with both *HOXA1* and *HOXA3* interacting with *HOXA9*.

Source data are provided as a Source Data file.

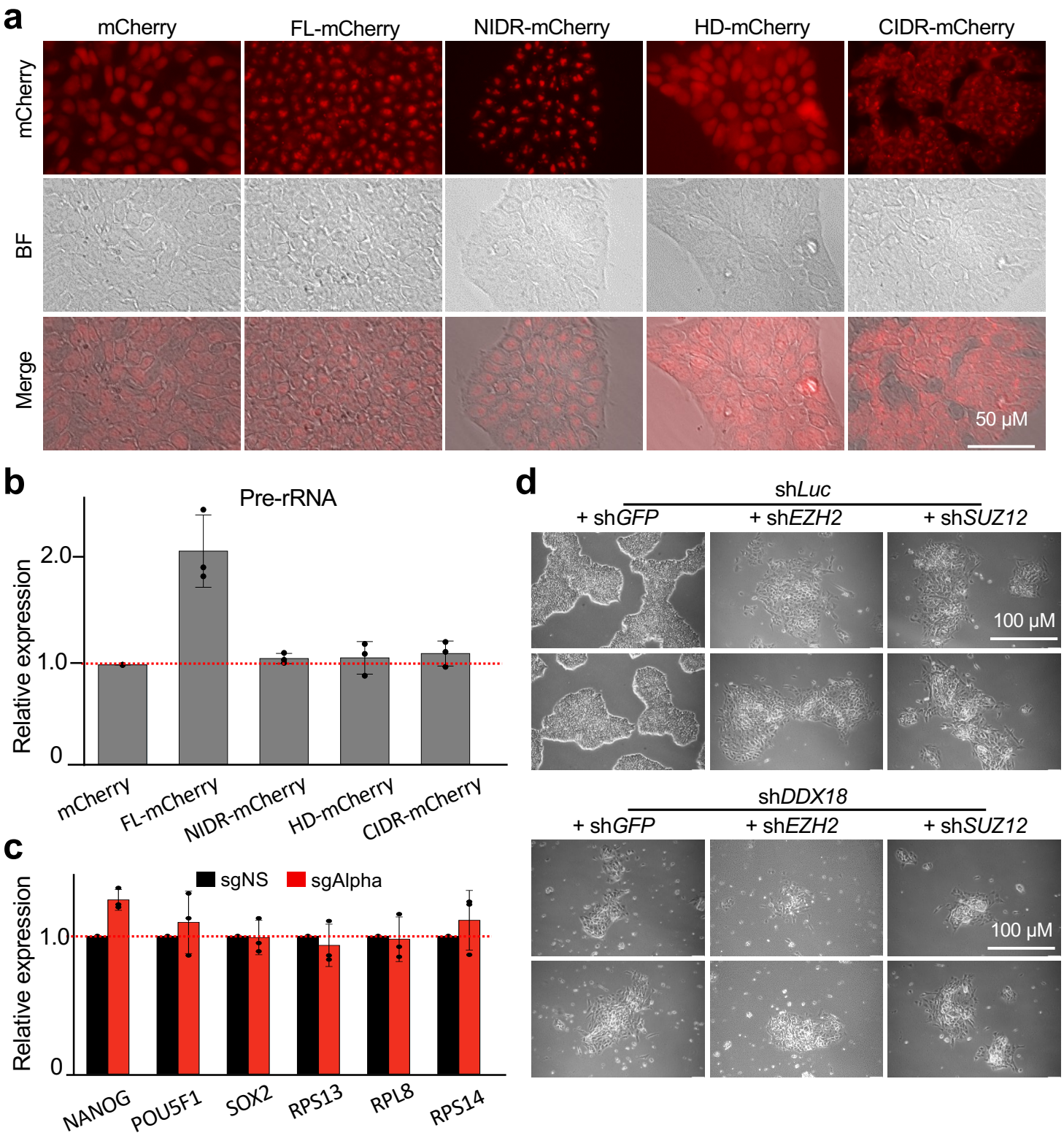
a
mCherry
FL-mCherry
NIDR-mCherry
HD-mCherry
CIDR-mCherry
mCherry
BF
Merge
50 μM
b
Pre-rRNA
Relative expression
2.0
1.0
0
mCherry
FL-mCherry
NIDR-mCherry
HD-mCherry
CIDR-mCherry
c
sgNS
sgAlpha
Relative expression
1.0
0
NANOG
POU5F1
SOX2
RPS13
RPL8
RPS14
d
shLuc
+ shGFP
+ shEZH2
+ shSUZ12
100 μM
shDDX18
+ shGFP
+ shEZH2
+ shSUZ12
100 μM

Supplementary Fig. S7 | NoCasDrop of DDX18 restructures the genome positioning and controls gene expression.

a, Live-cell imaging of nucleolus localization by dCas9-mCherry fused with full-length (FL) DDX18 or its truncated domains (NIDR, HD, CIDR) in human ESCs.

b, RT-qPCR analysis showing DDX18 FL increases pre-rRNA production.

c, RT-qPCR analysis showing NoCasDrop does not affect the expression of pluripotency genes or ribosomal protein genes.

d, Phase-contrast images showing that hESC differentiation by DDX18 KD cannot be rescued by depletion of PRC2 gene *EZH2* or *SUZ12*.

Source data are provided as a Source Data file.

Additional References

1. Gifford, C.A. *et al.* Transcriptional and epigenetic dynamics during specification of human embryonic stem cells. *Cell* **153**, 1149-1163 (2013).
2. Tanaka, Y. *et al.* Transcriptome Signature and Regulation in Human Somatic Cell Reprogramming. *Stem Cell Reports* **4**, 1125-1139 (2015).
3. Tsankov, A.M. *et al.* Transcription factor binding dynamics during human ES cell differentiation. *Nature* **518**, 344-349 (2015).
4. Meuleman, W. *et al.* Constitutive nuclear lamina-genome interactions are highly conserved and associated with A/T-rich sequence. *Genome Res* **23**, 270-280 (2013).